# Structure and properties of $Ba_9Fe_3S_{15}$ with quasi-one-dimensional spin chains

Jun Zhang,[1,2,*] Yating Jia,[3,*] Xiaoming Chen,[1,4] Baosen Min,[1,2] Takashi Honda,[5] Zhiwei Hu,[6] Liu Hao Tjeng,[6] Shin-ichi Shamoto,[5,7] Jianfa Zhao,[1] Zheng Deng,[1] Jing Song,[1] Lei Duan,[4] Manuel Valvidares,[8] Jinlong Zhu,[9] Xiancheng Wang,[1,2,†] and Changqing Jin[1,2,‡]

[1]*Beijing National Laboratory for Condensed Matter Physics, Institute of Physics, Chinese Academy of Sciences, Beijing 100190, China*
[2]*School of Physics, University of Chinese Academy of Sciences, Beijing 100190, China*
[3]*Quantum Science Center of Guangdong–Hong Kong–Macao Greater Bay Area (Guangdong), Shenzhen 518045, China*
[4]*School of Materials Science and Engineering, Henan University of Technology, Zhengzhou 450007, China*
[5]*Institute of Materials Structure Science, High Energy Accelerator Research Organization (KEK), Tsukuba, Ibaraki 305-0801, Japan*
[6]*Max Plank Institute for Chemical Physics of Solids, Nöthnitzer Straβe 40, D-01187 Dresden, Germany*
[7]*Neutron Science and Technology Center, Comprehensive Research Organization for Science and Society (CROSS), Tokai 319-1106, Japan*
[8]*ALBA Synchrotron Light Source, E-08290 Cerdanyola del Vallès, Barcelona, Spain*
[9]*Department of Physics, Southern University of Science and Technology, Shenzhen 518055, China*

(Received 26 February 2025; revised 13 May 2025; accepted 16 May 2025; published 3 June 2025)

In this work, the properties of $Ba_9Fe_3S_{15}$ have been studied via magnetism, electrical transport, and specific heat measurements. The crystal structure mainly consists of face-sharing octahedral $FeS_6$ chains with an interchain distance of 9.2320 Å, demonstrating a strongly quasi-one-dimensional (1D) character. $Ba_9Fe_3S_{15}$ is a semiconductor with a band gap of 562 meV and its electrical transport property is dominated by $p$ electrons. The semiconducting behavior is kept under the highest pressure up to 62 GPa. The long-range spin order (LRSO) transition has been observed with $T_C \sim 8.8$ K. The neutron diffraction experiments provide evidence that $Ba_9Fe_3S_{15}$ hosts ferrimagnetic spin chains with the spins parallel to (110) and the spin assignment of $Fe_2 \uparrow Fe_1 \downarrow Fe_2 \uparrow$. $T^{0.5}$ dependence on the magnetic contribution to the specific heat has been observed above $T_C$, indicating the natural property of the 1D ferrimagnetic spin chain. In addition, the magnetic susceptibility deviates from the Curie-Weiss law far above $T_C$, and the LRSO transition only causes a small kink in the specific heat curve; these imply that short-range spin orders have formed above $T_C$ because of the strong intrachain spin coupling. Also, it is revealed that the ordered moment is reduced by over 40% in $Ba_9Fe_3S_{15}$, which is indicative of the spin partially ordered state below $T_C$ and implies the existence of strong quantum fluctuation in the reduced dimension system. $Ba_9Fe_3S_{15}$ should be a unique example to further study the intrinsic properties of an ideal ferrimagnetic spin chain.

DOI: 10.1103/PhysRevB.111.224405

## I. INTRODUCTION

Iron based compounds have attracted much attention since LaFeAs(O,F) was reported to have superconductivity (SC) with $T_C \sim 26$ K [1,2]. For the main iron based superconductors, such as LnOFeAs [2–5], $(Ba,K)Fe_2As_2$ [6], LiFeAs [7], and FeSe [8], the FeAs/Se layers formed by edge-sharing tetrahedral $FeAs/Se_4$ play a key role for their SC. Besides the layered iron based superconductors, it is interesting that SC has been observed in iron chalcogenides of $BaFe_2S_3$ and $BaFe_2Se_3$ under high pressure [9–11]. The crystal structure of these compounds consists of edge-sharing tetrahedral $FeS/Se_4$ spin ladders aligned along the $c$ axis. $BaFe_2S_3$ is a Mott insulator that exhibits a stripe-type antiferromagnetic ordering below 120 K [9], while for $BaFe_2Se_3$, it has been reported to possess a block-type antiferromagnetic structure with a Néel temperature ($T_N$) of 256 K [12]. After the antiferromagnetism is suppressed by pressure, $BaFe_2S_3$ and $BaFe_2Se_3$ exhibit SC with a $T_C$ of approximately 24 K [10] and 11 K [11], respectively. It seems that the SC can be realized in iron based compounds with diverse structural motifs. Therefore, we are motivated to explore SC in other iron chalcogenides that feature one-dimensional (1D) spin chains.

Recently, we have discovered a series of quasi-1D compounds, $Ba_3MX_5$ [13–18] ($M$ denotes a $3d$ transition metal and $X$ is chalcogen), of which the crystal structure consists of face-sharing octahedral $MX_6$ chains. Among these quasi-1D compounds, $Ba_9Fe_3Te_{15}$ hosts antiferromagnetic spin chains [14] and demonstrates SC with $T_C \sim 4.7$ K under a pressure of 26 GPa [19], while $Ba_9Fe_3Se_{15}$ undergoes a ferromagnetiklike long-range spin order (LRSO) transition at 14 K and changes from semiconductor to metal at 29 GPa accompanied by a spin state crossover from a high-spin to a low-spin state [15]. $Ba_9Fe_3S_{15}$ is an early reported material synthesized by Jenks *et al.* in 1978, and only the crystal structure has been studied in the previous work [20]. Here, we report the physical properties of $Ba_9Fe_3S_{15}$ related to its quasi-1D structure in

*These authors contributed equally to this work.
†Contact author: wangxiancheng@iphy.ac.cn
‡Contact author: jin@iphy.ac.cn

 

detail. $Ba_9Fe_3S_{15}$ behaves like a semiconductor and *p* electrons dominate its transport property. No pressure-induced semiconductor-metal transition has been observed up to 62 GPa. It is ferrimagnetic with the LRSO transition temperature $T_C \sim 8.8$ K, above which $T^{0.5}$ dependence on magnetic contribution to the specific heat has been observed. Our results indicate that $Ba_9Fe_3S_{15}$ is a typical example with quasi-1D ferrimagnetic spin chains.

## II. EXPERIMENTS

$Ba_9Fe_3S_{15}$ was synthesized at high-pressure and high-temperature conditions. Initially, a precursor of BaS was prepared by heating the Ba blocks and S powder in an $Al_2O_3$ tube sealed in an evacuated quartz tube at 600 °C for 10 h. A mixture of BaS, Fe, and S powders with stoichiometric ratio of 3:1:2 was ground and pressed into a pellet with a diameter of 6 mm, and then sintered at 1200 °C under 5.5 GPa for 30 min, after which the black polycrystalline sample of $Ba_9Fe_3S_{15}$ was obtained.

Powder x-ray diffraction (XRD) was performed on a Rigaku Ultima VI (3 KW) diffractometer using Cu $K\alpha$ radiation generated at 40 kV and 40 mA. The data were collected at a scanning rate of 1 °/min with a scanning step length of 0.02°. The Rietveld refinement on the diffraction spectra was conducted with the GSAS and EXPGUI packages [21]. The dc magnetic susceptibility was measured using a superconducting quantum interference device (SQUID). The electronic transport and specific heat were measured at ambient pressure by using a physical property measurement system (PPMS). The neutron powder diffraction (NPD) experiments were performed with high intensity total diffractometer (NOVA) installed in the Materials and Life Science Experimental Facility (MLF) of the Japan Proton Accelerator Research Complex (J-PARC). Soft *x*-ray absorption spectroscopy (XAS) and the Fe-$L_{2,3}$ x-ray magnetic circular dichroism (XMCD) experiments were performed at the BOREAS undulator beamline of the ALBA synchrotron light source near Barcelona [22].

The *in situ* high-pressure resistance measurements were carried out in a MagLab system which provides low-temperature conditions. The diamond anvil cell (DAC) technique was adopted for generating high pressure. The culet of diamond anvils is 300 μm in diameter. T301 stainless steel was used as the gasket; cubic BN serves as the insulating layer and NaCl fine powder as the pressure-transmitting medium. The pressure was calibrated by the ruby fluorescence method. High-pressure synchrotron XRD experiments were performed at the Beijing Synchrotron Radiation Facility at room temperature with a wavelength of 0.6199 Å using a symmetric DAC. Silicon oil was loaded as the pressure-transmitting medium for these experiments. The details of *in situ* high-pressure experiments can be seen in Refs. [23–25].

## III. RESULTS

Figure 1(a) displays the XRD pattern of the $Ba_9Fe_3S_{15}$ powder sample. The refinement was carried out by adopting the initial structural model of $Ba_9Fe_3S_{15}$ with the space group of $P\bar{6}c2$ reported by Jenks [20], which smoothly converges to $\chi^2 = 3.0$, $R_p = 2.3\%$, $wR_p = 3.4\%$ and confirms the high

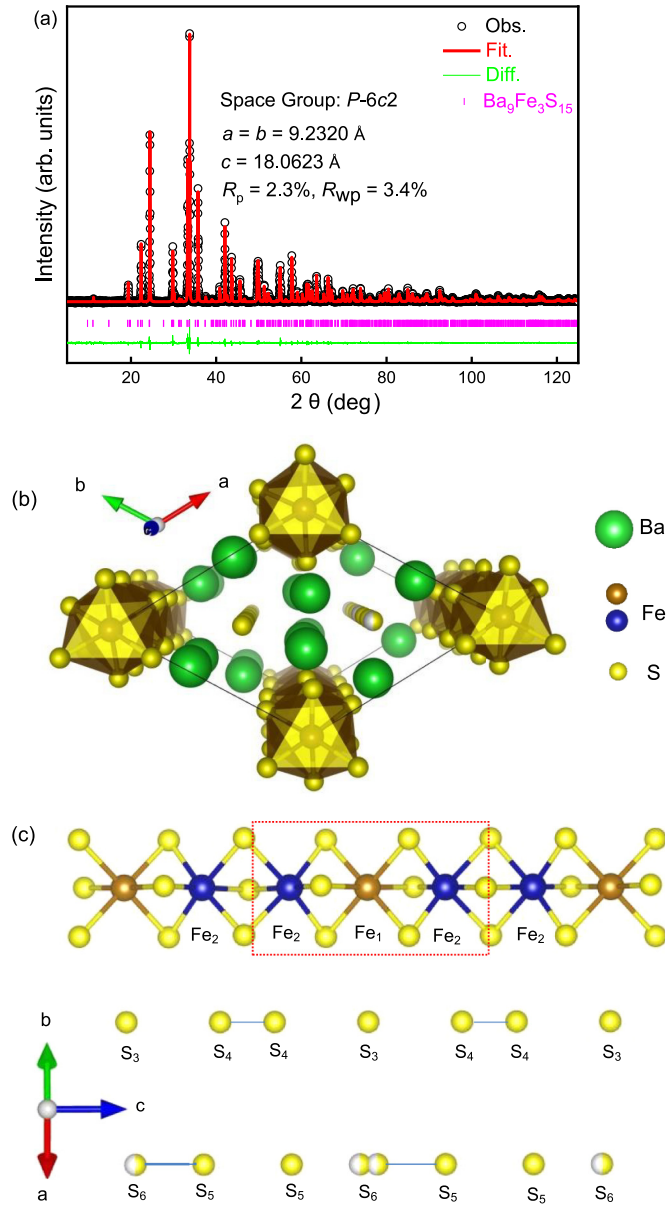


FIG. 1. (a) The x-ray diffraction pattern and the refinement for $Ba_9Fe_3S_{15}$ sample. (b) The crystal structure of $Ba_9Fe_3S_{15}$ projected along [001]. (c) The nonuniform Fe chains and S chains in the trimerized structure of $Ba_9Fe_3S_{15}$.

quality of our sample. The lattice constants are $a = b = 9.2320$ Å and $c = 18.0623$ Å, agreeing with the previous results [20]. The crystal structure of $Ba_9Fe_3S_{15}$ projected along [001] is sketched in Fig. 1(b). $Ba_9Fe_3S_{15}$ mainly consists of face-sharing octahedral $FeS_6$ chains running along the *c* axis. The $FeS_6$ chains are arranged in a triangular lattice in the *ab* plane with a large distance more than 9.0 Å; thus $Ba_9Fe_3S_{15}$ demonstrates strong 1D spin-chain character. Beside the $FeS_6$ chains, two S chains are located in the centers of the triangular lattices with the sites of (1/3, 2/3, *x*) and (2/3, 1/3, *y*). In addition, as shown in Fig. 1(c), the structure is trimerized in the direction of the *c* axis, leading to nonuniform $FeS_6$ chains and S chains which are composed of $Fe_1$ and $Fe_2$ atoms, $S_3$ and $S_4$ atoms, and $S_5$ and $S_6$ atoms, respectively.

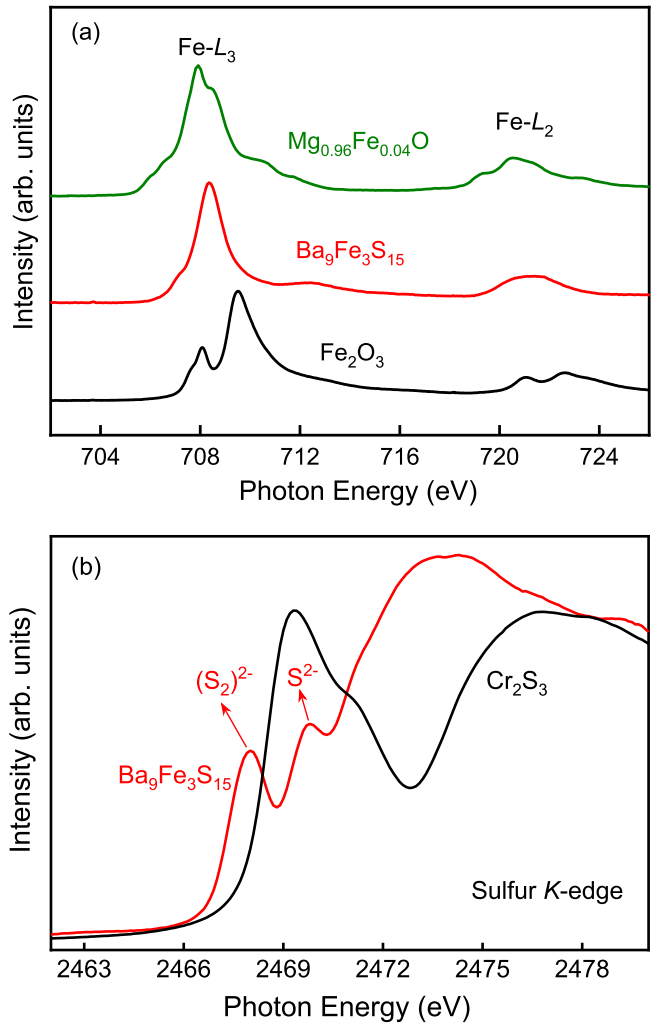


FIG. 2. (a) The soft XAS spectrum of $Ba_9Fe_3S_{15}$ at the Fe-$L_{2,3}$ edge and those of $Fe_2O_3$ and $Mg_{0.96}Fe_{0.04}O$ as $Fe^{3+}$ and $Fe^{2+}$ reference materials. (b) The sulfur $K$-edge XAS spectrum of $Ba_9Fe_3S_{15}$ with $Cr_2S_3$ as the reference material.

For the sites occupied by the $Se_6$ atoms, the occupation ratio is 0.5. In the S chains, the distance of $S_4 - S_4$, $S_3 - S_4$, $S_5 - S_6$, and $S_5 - S_5$ are 2.5616, 3.2347, 2.0638, and 3.7956 Å, respectively. It is indicated that covalent bonds should have formed between the adjacent $S_4 - S_4$ and $S_5 - S_6$ atoms as reported in our previous works for its sister compounds of $Ba_9Fe_3Se_{15}$ [15] and $Ba_9Fe_3Te_{15}$ [14].

To investigate the oxidation state of iron atoms in $Ba_9Fe_3S_{15}$, we conducted soft XAS measurements, which are very sensitive to the valence state [26,27] and the local environment [28,29]. Figure 2(a) shows the XAS spectrum of $Ba_9Fe_3S_{15}$ at the Fe-$L_{2,3}$ edge and those of $Fe_2O_3$ and $Mg_{0.96}Fe_{0.04}O$ as $Fe^{3+}$ and $Fe^{2+}$ reference materials, respectively. The main peak in the $Ba_9Fe_3S_{15}$ spectrum is almost at the same photon energy as that of $Mg_{0.96}Fe_{0.04}O$, while the photon energy is ∼1.2 eV smaller than that of $Fe_2O_3$, demonstrating that the valence state for Fe ions in $Ba_9Fe_3S_{15}$ should be 2+. Also, the sulfur $K$-edge XAS spectrum for the $Ba_9Fe_3S_{15}$ sample with $Cr_2S_3$ as the reference material has been collected as shown in Fig. 2(b). For $Ba_9Fe_3S_{15}$, there are two peaks for sulfur $K$-edge absorption centering at 2468.01 and 2469.77 eV corresponding to S-S bonding and Fe-S bonding, respectively. Two such peaks for sulfur $K$-edge absorption have also been observed in $Ba_6Cr_2S_{10}$ with dimerized structure [13], which further confirms the formation of sulfur pairs of $(S_2)^{2-}$ and the nonuniform character of the S chain in $Ba_9Fe_3S_{15}$.

Figure 3(a) presents the temperature dependence of magnetic susceptibility $\chi(T)$ for $Ba_9Fe_3S_{15}$ with applied magnetic field $H = 500$ Oe. The curves of zero field cooling (ZFC) and field cooling (FC) overlap each other in the measured temperature range, and display a ferromagnetlike transition at low temperature. In fact, it is a ferrimagnetic transition as will be proved in the following neutron experiments. The temperature derivative of susceptibility, $d\chi/dT$, was plotted as seen in the inset of Fig. 3(a), and the Curie temperature $T_C$ was determined to be 8.8 K. The magnetic hysteresis loop measured at 1.8 K is shown in Fig. 3(b). The magnetization increases sharply when initially increasing $H$ and becomes saturated with the saturated moment $\mu_{sat}$ about 1.2 $\mu_B$/Fe when $H = 7$ T. As shown in the inset of Fig. 3(b), the magnetic coercivity is less than 15 Oe; this is why the ZFC and FC $\chi(T)$ curves measured at 500 Oe are totally overlapped. Figure 3(c) displays the inverse of susceptibility, $1/\chi$, versus temperature. Obviously, the temperature dependence of $\chi(T)$ deviates from the Curie-Weiss law below 120 K. After the $1/\chi(T)$ data within the temperature range from 200 to 300 K are fitted by a straight line, we can obtain the effective moment $\mu_{eff} = 7.1\mu_B$/Fe and the Curie-Weiss temperature $T_\theta = 155$ K. Both the obtained values of $\mu_{eff}$ and $T_\theta$ are much larger than the expected value of $\mu_{eff}$ for $Fe^{2+}$ with high-spin state ($S = 2$) and the ordering temperature $T_C$, respectively.

To further study the magnetic property of the Fe ions in $Ba_9Fe_3S_{15}$, we collected the Fe-$L_{2,3}$ x-ray magnetic circular dichroism (XMCD) spectra of $Ba_9Fe_3S_{15}$ at 2 K and 6 T, using circularly polarized x-rays with the photon spin parallel [$\sigma+$ (black line)] and antiparallel [$\sigma-$ (red line)] to the applied magnetic field, respectively, as seen in Fig. 3(d). The difference spectrum, x-ray magnetic circular dichroism (XMCD), is denoted with the blue line. The sum rules developed by Thole *et al.* [30] and Carra *et al.* [31] are used to determine the ratio between the orbital $m_{orb} = L_z$ and spin $m_{spin} = 2S_z$ contributions to the magnetic moment, namely,

$$\frac{L_z}{2S_z + 7T_z} = \frac{2}{3}\frac{\int_{L_{2,3}}(\sigma^+ - \sigma^-)dE}{\int_{L_3}(\sigma^+ - \sigma^-)dE - 2\int_{L_2}(\sigma^+ - \sigma^-)dE},$$

where the magnetic dipole moment $T_z$ for ions in octahedral symmetry is small relative to $S_z$ and can be neglected. By using sum rules, the moment ratio $m_{orb}/m_{spin}$ can be obtained to be ∼0.2. Therefore, the orbital moment $m_{orb}$ should be ∼0.8 $\mu_B$ if assuming $S = 2$ for $Fe^{2+}$ in the high-spin state. Thus the total moment of the $Fe^{2+}$ ion is 4.8 $\mu_B$ with a sizable unquenched orbital moment. By using the obtained orbital momentum, we can calculate the $g$ factor to be ∼1.71 and then the effective moment $\mu_{eff} \sim 5.58$ $\mu_B$ via the equation of $\mu_{eff} = g\sqrt{J(J+1)}$, where $J = 2.8$ $\mu_B$ is the sum of $L$ and $S$. The expected effective moment is still much smaller than the estimated value of 7.1 $\mu_B$ from $\chi(T)$ data although the

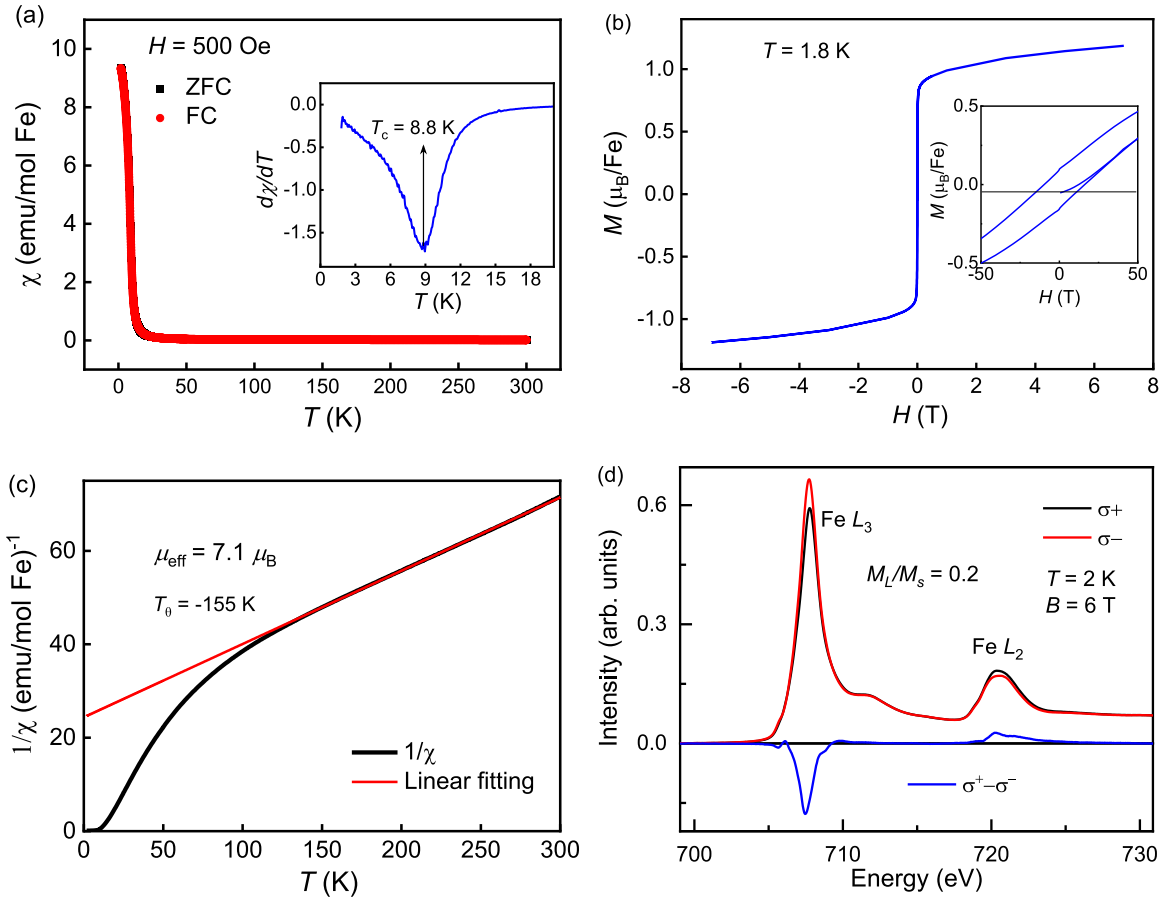


FIG. 3. (a) The temperature dependence of magnetic susceptibility $\chi(T)$ for $Ba_9Fe_3S_{15}$ measured with $H = 500$ Oe. The inset is the temperature derivative $d\chi/dT$, showing the magnetic transition temperature $T_C$. (b) The magnetic hysteresis loop measured at 1.8 K. (c) The inverse of susceptibility $1/\chi$ vs temperature. The red line is the fitting according to Curie-Weiss law. (d) The Fe-$L_{2,3}$ XAS spectra of $Ba_9Fe_3S_{15}$ collected at 2 K and 6 T by using circularly polarized x-rays. The black and red lines are the spectra with the photon spin parallel ($\sigma+$) and antiparallel ($\sigma-$) to the applied magnetic field, respectively. The blue line denotes the difference spectrum XMCD.

contribution of the orbital moment is considered. It seems that the effective moment is overestimated by fitting the $\chi(T)$ data according to the Curie-Weiss law.

Figure 4(a) presents the specific heat data near $T_C$. Although there is only a small kink corresponding to the LRSO transition, the $T_C$ value can be determined to be ~8.8 K from the temperature derivative of the specific heat curve, which agrees with the value that has been obtained from magnetic susceptibility measurements. For a quasi-1D spin-chain system, the spin chains would be decoupled above the LRSO temperature and can be considered as ideal spin chains. As the following results from NPD experiments show, $Ba_9Fe_3S_{15}$ hosts ferrimagnetic spin chains, where the magnetic contribution to specific heat $C_{mag}$ due to the spin excitation is expected to be proportional to $T^{1/2}$ [32]. Therefore, we use the equation $C = \alpha T^{1/2} + \beta T^3 + \eta T^5$ to carry out the fit to the specific heat data above $T_C$, where the first term is the magnetic contribution $C_{mag}$ and the second and third terms are the lattice contribution. Here, the electron contribution to the specific heat is ignored because of the semiconducting feature of $Ba_9Fe_3S_{15}$. The fitting as shown with the red line in Fig. 4(a) gives the coefficients of $\alpha = 0.557\text{J}/(\text{Fe mol K}^{1.5})$ and $\beta = 0.002\text{J}/(\text{Fe mol K}^4)$. According to the formula $\theta_D = [(12/5)NR\pi^4/\beta n]^{1/3}$, where $N$ is the Avogadro constant, $R$ is the universal gas constant, and $n = 9$ is the atomic number of $Ba_3FeS_5$, the Debye temperature ($\theta_D$) of $Ba_9Fe_3S_{15}$ can be calculated to be 206 K. In addition, the large coefficient of $\alpha$ suggests an unambiguous magnetic contribution to the specific heat and is indicative of the 1D spin-chain character. The temperature dependence of $C_{mag}$ can be obtained by subtracting the lattice contribution from the heat specific data, and the magnetic entropy $S_{mag}$ can be estimated through the integration of $C_{mag}/T$ in the temperature range from 2 to 28 K. If ignoring the magnetic entropy change below 2 K, the $S_{mag}$ near $T_C$ is ~1.2 J/(Fe mol K), which is only ~8% of the expected value $R\ln(2J + 1) = 15.7$ J/mol K for a $J = 2.8$ system.

Figure 4(b) displays the temperature dependence of resistivity for $Ba_9Fe_3S_{15}$, which exhibits a semiconductor behavior. The $\ln(\rho)$ versus $1/T$ shows a straight line as shown in the inset of Fig. 4(b), implying the semiconductor should be an Arrhenius type. Using the formula $\rho \propto \exp(\Delta/2k_BT)$, where $\Delta$ is the semiconducting band gap and $k_B$ is Boltzmann's constant, the resistivity curve is fitted and the band gap $\Delta$ is obtained to be 562 meV. The resistivity curves for the sister compounds of both $Ba_9Fe_3Se_{15}$ and $Ba_9Fe_3Te_{15}$

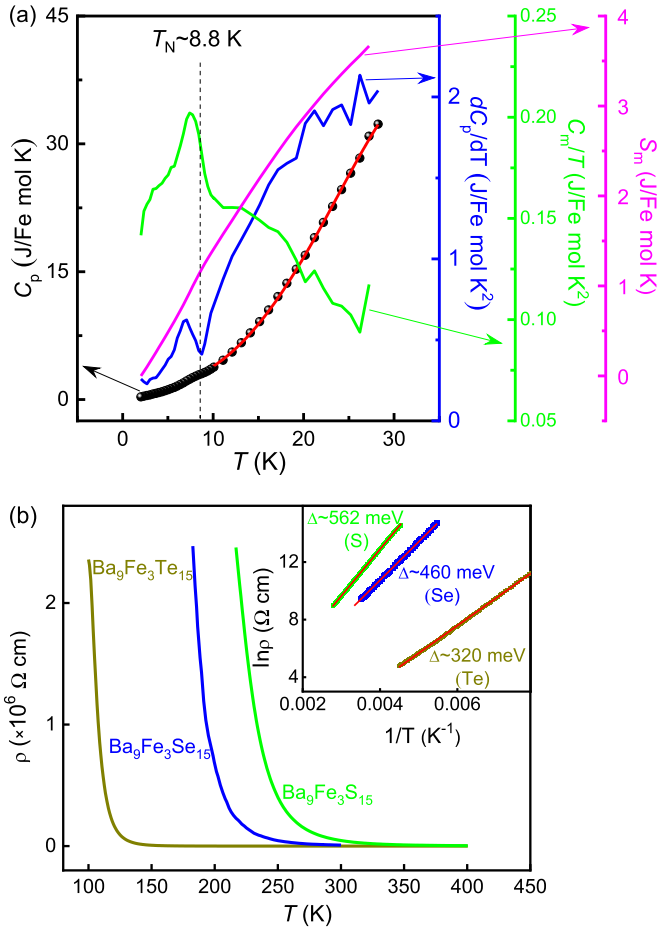


FIG. 4. (a) The specific heat data near the magnetic transition. The red line is the fitting using the equation $C = \alpha T^{1/2} + \beta T^3 + \eta T^5$. The blue curve is the temperature derivative of the specific heat curve, the green curve is the magnetic contribution to the specific heat divided by temperature, and the purple curve is the magnetic entropy. (b) The temperature dependence of resistivity measured at ambient pressure for $Ba_9Fe_3S_{15}$; the data of $Ba_9Fe_3Se_{15}$ and $Ba_9Fe_3Te_{15}$ are extracted from Refs. [14,15]. The inset shows the $\ln(\rho)$ vs $1/T$ and the fitting using the formula $\rho \propto \exp(\Delta/2k_BT)$.

are also shown in Fig. 4(b). The band gap Δ increases in the sequence of the compounds with the anions from Te, Se, and S.

In order to investigate the magnetic structure of $Ba_9Fe_3S_{15}$, we carried out the NPD measurements. The NPD patterns collected at 50 and 2 K are shown in Fig. 5(a). Clear differences between the two diffraction patterns are the enhancement of the peaks indexed as 212, 114, 104, 112, and 102, respectively, which should arise from the contribution of the magnetic lattice. Refinement using an irreducible representation analysis of the magnetic structure suggests that the magnetic moment of Fe should be in the *ab* plane. The structure parameter, irreducible representation analysis, and the allowed magnetic structures can be found in Tables S1–S3 and Fig. S1 in the Supplemental Material [33], respectively. The temperature dependence of the integrated intensity of the magnetic Bragg peak 102-Q is shown in Fig. 5(b), which further demonstrates that the LRSO happens at ~9 K. From the Rietveld refinement for the NPD pattern collected at 2 K, as seen in Fig. 5(c), the magnetic moment of $Fe_1$ at the 2*a* site is estimated to be 2.58 $\mu_B$ and that of $Fe_2$ at the 4*g* site is 2.80 $\mu_B$. The obtained magnetic structure is sketched in Fig. 5(d). The spins are aligned along the (110) direction, and ferromagnetically coupled in the *ab* plane while they are ferrimagnetically arranged along the *c* axis with the spin assignment of $Fe_2 \uparrow Fe_1 \downarrow Fe_2 \uparrow$. Thus the net ferromagnetically ordered moment should be ~1.01 $\mu_B$/Fe, which is consistent with the extrapolated value from high magnetic field magnetization to zero field in Fig. 3(b).

The structure stability and the resistance under pressure were investigated. Figure 6(a) shows the *in situ* high-pressure x-ray diffraction patterns for $Ba_9Fe_3S_{15}$. No new Bragg peak is observed up to 45.4 GPa, implying the crystal structure is stable within such a pressure range. The Bragg peaks gradually shift towards the high-angle direction when increasing pressure; this implies that the lattice has been compressed by pressure. Figure 6(b) presents the pressure dependence of lattice constants *a* and *c*. At 45.4 GPa, the values of *a* and *c* have been compressed by ~12% and ~16%, respectively. Figure 6(c) displays the ratio of *c*/*a* versus *P*. The decrease of the ratio of *c*/*a* with increasing pressure is indicative of the anisotropic compression under high pressure. In addition, there obviously exists a kink at ~30 GPa in the pressure dependence of *c*/*a*. It is speculated that such an anomaly should be related to an electronic transition. For the sister compound $Ba_9Fe_3Se_{15}$, a similar kink in the evolution of lattice constants tuned by pressure also has been reported and it is associated with a spin state transition from high-spin state to low-spin state [15]. Figure 6(d) presents the cell volume as a function of pressure. Using the Birch-Murnaghan equation,

$$P(\mathrm{GPa}) = \tfrac{3}{2} \times B_0[(V_0/V)^{\frac{7}{3}} - ((V_0/V))^{\frac{5}{3}}] \times \left\{1 - \left(3 - \tfrac{3}{4} \times B_0^{'}\right) \times [((V_0/V))^{\frac{2}{3}} - 1]\right\},$$

where the pressure derivative $B_0^{'}$ is fixed as 4, a fitting to the data up to 30 GPa gives the bulk modulus $B_0 = 47.1$ GPa.

The temperature dependence of resistance under different pressures is shown in Fig. 7(a) with the highest experimental pressure of 62.5 GPa. The resistance is gradually reduced by applying pressure and exhibits semiconducting behavior even at 62.5 GPa. In particular, at low temperature the resistance is sharply reduced by nearly five orders of magnitude when pressure increases from 24.1 to 31.2 GPa. We plotted the pressure dependence of resistance at different fixed temperatures as shown in Fig. 7(b). It is clearly seen that the slope of *dR*/*dP* changes dramatically at ~31 GPa, which is consistent with the value where a kink is observed in the curve of *c*/*a* as a function of pressure; this further suggests an electronic transition occurs at this pressure. The *in situ* high-pressure resistance measurements on a second sample were performed as shown in Figs. S2(a) and S2(b) [33]. The behavior of resistance dependent on pressure is similar to that in Fig. 7(b). That is, the change of the slope of *dR*/*dP* can be reproduced, confirming the possible electronic transition.

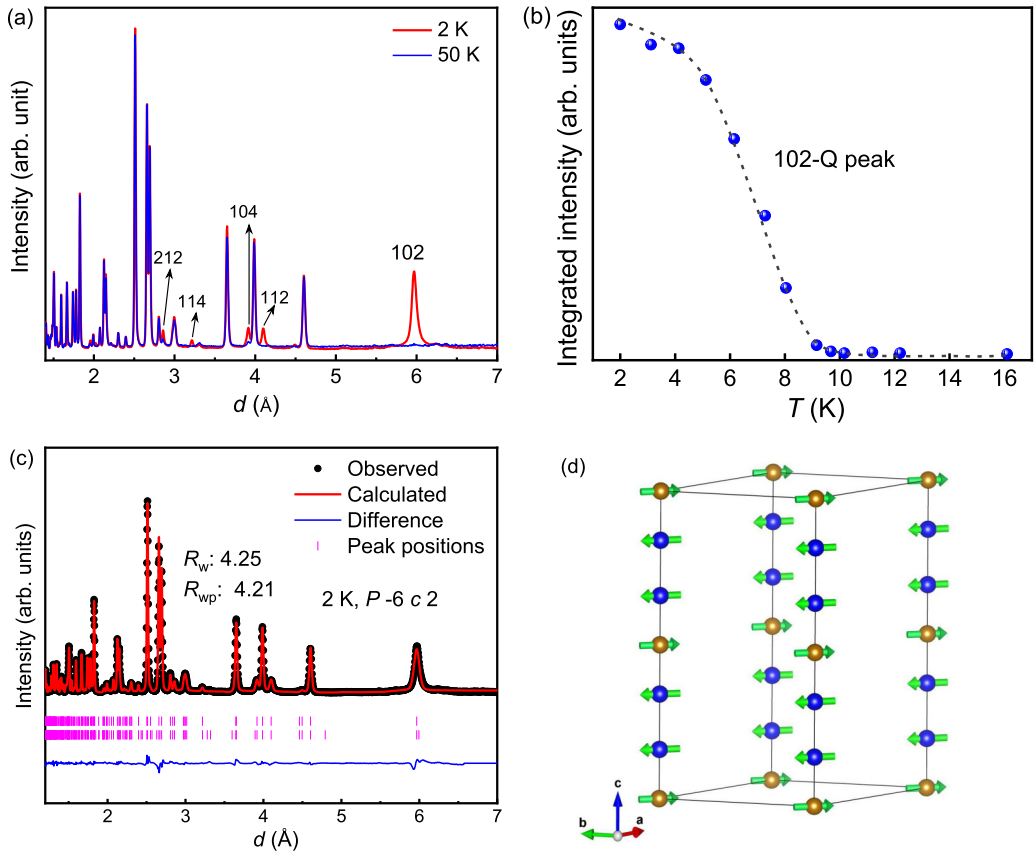


FIG. 5. (a) The NPD patterns collected at 50 and 2 K for $Ba_9Fe_3S_{15}$. (b) The temperature dependence of integrated intensity for the magnetic Bragg peak 102-Q. (c) The refinement for the NPD patterns collected at 2 K. (d) The magnetic structure of $Ba_9Fe_3S_{15}$ obtained from the refinement of the NPD pattern collected at 2 K.

## IV. DISCUSSIONS

In the sequence of $X$ = S, Se, and Te, $Ba_9Fe_3X_{15}$ hosts ferrimagnetic spin chains, helical spin chains [34], and antiferromagnetic spin chains [14], respectively. Although the crystal structure of $Ba_9Fe_3Se_{15}$ was reported to be monoclinic ($C2/c$), slightly different from the hexagonal structure of $Ba_9Fe_3S_{15}$ and $Ba_9Fe_3Te_{15}$ ($P$-6$c$2) [15], the space group of $C2/c$ is centrosymmetric. That is, the helical spin structure might not be caused by the Dzyaloshinskii-Moriya (DM) interaction but might arise from the magnetic frustration, i.e., the competition between nearest neighbor (NN) spin coupling and the next nearest neighbor (NNN) spin coupling. It seems that the delocalization of $p$ electrons would have significant influence on the competition between NN and NNN interaction and lead to different magnetic ground states. It is warranted to further study the role of varying anion or applying high pressure on the magnetic ground state of $Ba_9Fe_3X_{15}$ in the future.

$Ba_9Fe_3S_{15}$ features strong quasi-1D spin chains and S chains. In the system of $Ba_9Fe_3X_{15}$ with $X$ = S, Se, and Te, the band gap of $Ba_9Fe_3X_{15}$ increases in sequence when the anion varies from Te to Se and to S although the lattice constants shrink, which suggests that the $p$-orbital electrons dominate the transport properties. Such phenomena have been observed in many other systems with quasi-1D structure. In the compounds of $Ba_9Co_3(Se_{1-x}S_x)_{15}$ ($x \leqslant 0.2$), which has a similar quasi-1D structure to $Ba_9Fe_3X_{15}$, the resistivity has been reported to gradually increase with increasing the S doping level [35]. Another typical example is $BaVS/Se_3$ with face-sharing octahedral $VS/Se_6$ chains, where $BaVS_3$ has an insulating ground state while $BaVSe_3$ is metallic and considered as the high-pressure counterpart of $BaVS_3$ [36–38]. Actually, for a quasi-1D conducting chain system, the transport property is governed by the electron hopping among the chains. When the electron hopping is small, the 1D conducting chains should be translated to insulators due to the umklapp scattering effect within the chain. Since the $p$ electrons with low quantum number orbital are more localized than those with high quantum number orbital, the variation of anion from Te to Se and to S should lead to the reduction of electron hopping between $FeX_6$ chains and result in an increase of the band gap.

$Ba_9Fe_3S_{15}$ also presents strong 1D spin-chain physics. For an ideal 1D spin chain, no LRSO can exist at finite temperature as implied by the Mermin-Wagner theorem due to strong quantum fluctuation [39]. However, in a quasi-1D spin-chain system there are two energy scales, i.e., interchain spin coupling strength $J_{inter}$ and intrachain coupling $J_{intra}$. Although $J_{inter}$ is typically two or three orders of magnitude lower than $J_{intra}$, the former usually governs the LRSO formation, before which SRSOs associated with large $J_{intra}$ have already

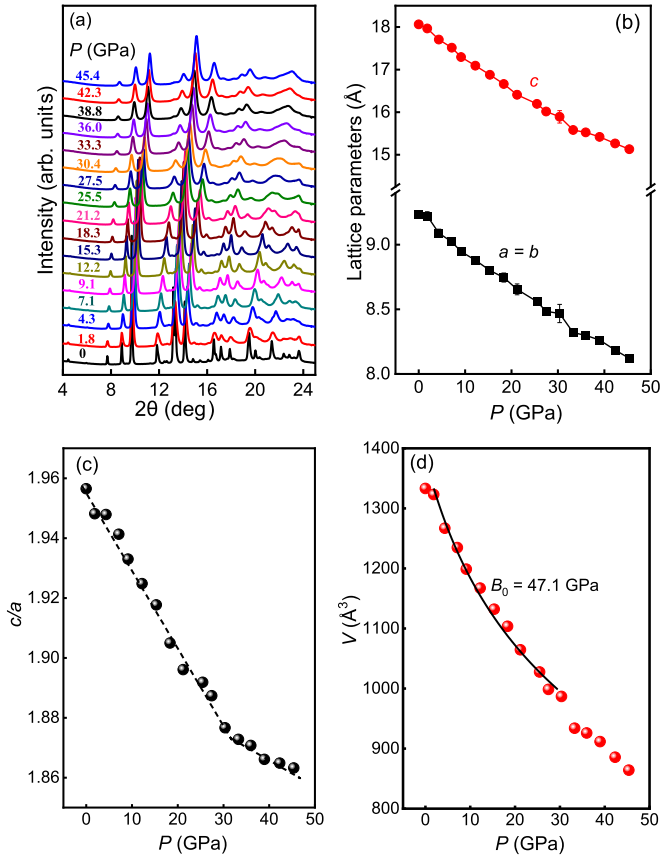


FIG. 6. (a) The *in situ* high-pressure x-ray diffraction patterns for $Ba_9Fe_3S_{15}$. (b) The pressure dependence of lattice constants $a$ and $c$. (c) The ratio of $c/a$ vs pressure. (d) The cell volume as a function of pressure. The black line is the fitting using the Birch-Murnaghan equation.

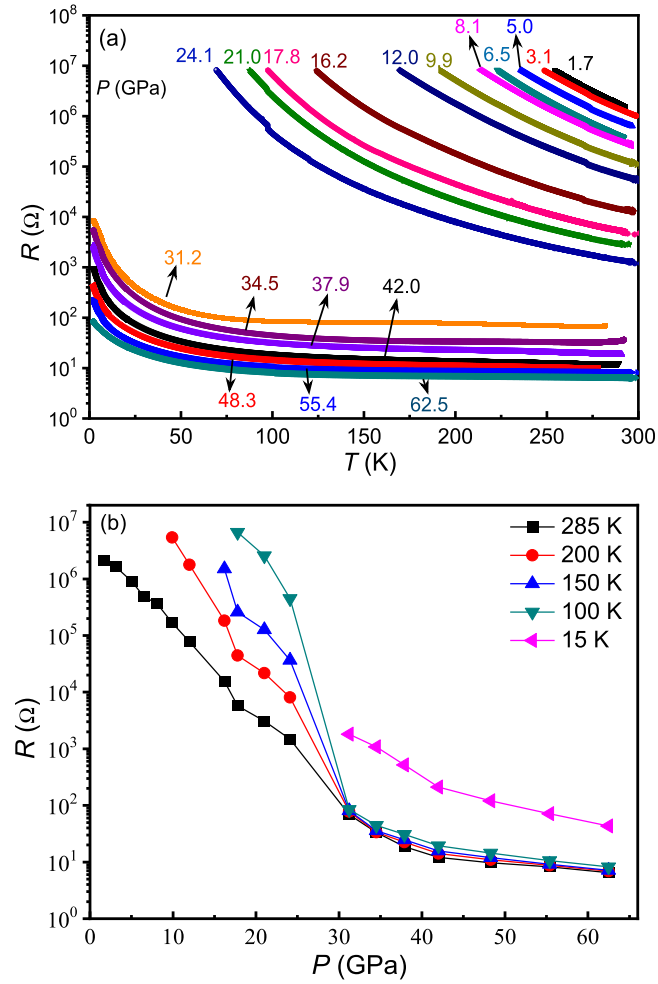


FIG. 7. (a) The temperature dependence of resistance under different pressures. (b) The pressure dependence of resistance at several fixed temperatures.

formed in the decoupled spin chains. The development of SRSOs above the LRSO temperature usually leads to rich exotic physics. For $Ba_9Fe_3S_{15}$, the Curie-Weiss temperature $T_\theta$ is much larger than the LRSO temperature $T_C$. Usually, the large disparity between $T_\theta$ and $T_C$ can be found in magnetic frustrated systems [40,41]. Here, the large $T_\theta$ value relative to $T_C$ is indicative of its quasi-1D spin-chain nature, where $T_\theta$ and $T_C$ are closely related with $J_{intra}$ and $J_{inter}$, respectively. Furthermore, below the Curie-Weiss temperature $T_\theta$, it is obvious that the slope of $1/\chi(T)$ gradually increases with decreasing temperature and the $\chi(T)$ deviates from the Curie-Weiss law. These phenomena have also been reported in the $Ba_9Fe_3Se_{15}$ compound [15]. Since our neutron diffraction evidences a ferrimagnetic state at low temperature for $Ba_9Fe_3S_{15}$, the SRSOs in the decoupled spin chains would gradually develop when decreasing temperature, leading to the decrease of effective moment and thus the increase of the slope of $1/\chi(T)$. In addition, in the specific heat curve as seen in Fig. 4(a), the small kink corresponding to the LRSO transition also is considered to arise from the formation of SRSOs, because most of the magnetic entropy would have been already released above the LRSO temperature. The magnetic entropy change above $T_C$ is estimated to be about 92% of the expected value of 15.7 J/mol K in this system.

Another phenomenon associated with quasi-1D spin chains is the reduced ordered moments because of reduced dimensions [42–44]. For such a system with a quasi-1D spin chain, there still exist a lot of SRSOs in the LRSO state due to the strong quantum fluctuation; this would lead to the reduction of ordered moments. For $KCuF_3$, a typical compound with quasi-1D spin chains, a saturated moment of 0.5 $\mu_B/Cu^{2+}$ was reported with a 50% reduction relative to the fully ordered moment for $Cu^{2+}$ ($S = 1/2$) [44]. Here, for $Ba_9Fe_3S_{15}$, the ordered moment obtained from neutron diffraction experiments collected at 2 K is 2.58 $\mu_B$ for Fe1 and 2.77 $\mu_B$ for Fe2, which is reduced over 42% compared with the expected total moment of 4.8 $\mu_B$ per $Fe^{2+}$. In our previous studies about the compounds with similar structure to $Ba_9Fe_3S_{15}$, a reduced ordered moment by ~65% has also been evidenced for $Ba_9V_3Te_{15}$ [17] and ~67% for $Ba_6Cr_2S_{10}$ [13]. These phenomena of reduction of ordered moment suggest strong quantum fluctuation existing in these systems.

## V. CONCLUSION

In summary, $Ba_9Fe_3S_{15}$ has a strong quasi-1D structure character. It exhibits a semiconducting behavior and the

$p$ electrons dominate the electrical transport property. The structure of $Ba_9Fe_3S_{15}$ is stable up to 45 GPa, and no semiconductor-metal transition has been observed even at the highest experimental pressure of 62 GPa. $Ba_9Fe_3S_{15}$ undergoes a ferrimagnetic transition at $T_C \sim 8.8$ K, above which unambiguous magnetic contribution with a characteristic $T^{0.5}$ dependence of the specific heat has been identified. $Ba_9Fe_3S_{15}$ hosts well-separated ferrimagnetic spin chains with the spin assignment of $Fe_2 \uparrow Fe_1 \downarrow Fe_2 \uparrow$, exhibits typical quasi-1D spin-chain physics with a sizable unquenched orbital moment of 0.8 $\mu_B$, and provides a good opportunity to further study the intrinsic physical properties of an ideal 1D ferrimagnetic chain.

## ACKNOWLEDGMENTS

This work was supported by the National Natural Science Foundation of China (Grant No. 12474097), the National Key R&D Program of China (Grants No. 2023YFA1406000 and No. 2024YFA1408000). The authors gratefully acknowledge the use of resources at the 4W2 beamline of the Beijing Synchrotron Radiation Facility (BSRF). The neutron total scattering experiment was approved by the Neutron Scattering Program Advisory Committee of IMSS, KEK (Proposal No. 2019S06).

## DATA AVAILABILITY

The data that support the findings of this article are not publicly available upon publication because it is not technically feasible and/or the cost of preparing, depositing, and hosting the data would be prohibitive within the terms of this research project. The data are available from the authors upon reasonable request.

[1] G. R. Stewart, Superconductivity in iron compounds, Rev. Mod. Phys. **83**, 1589 (2011).

[2] Y. Kamihara, T. Watanabe, M. Hirano, and H. Hosono, Iron-based layered superconductor La[$O_{1-x}F_x$]FeAs ($x = 0.05 - 0.12$) with $T_c = 26$ K, J. Am. Chem. Soc. **130**, 3296 (2008).

[3] Z. A. Ren, W. Lu, J. Yang, W. Yi, X. L. Shen, Z. C. Li, G. C. Che, X. L. Dong, L. L. Sun, F. Zhou, and Z. X. Zhao, Superconductivity at 55 K in iron-based F-doped layered quaternary compound Sm($O_{1-x}F_x$)FeAs, Chin. Phys. Lett. **25**, 2215 (2008).

[4] C. Wang, L. J. Li, S. Chi, Z. W. Zhu, Z. Ren, Y. K. Li, Y. T. Wang, X. Lin, Y. K. Luo, S. A. Jiang, X. F. Xu, G. H. Cao, and Z. A. Xu, Thorium-doping-induced superconductivity up to 56 K in $Gd_{1-x}Th_xFeAsO$, Europhys. Lett. **83**, 67006 (2008).

[5] X. H. Chen, T. Wu, G. Wu, R. H. Liu, H. Chen, and D. F. Fang, Superconductivity at 43 K in $SmFeAsO_{1-x}F_x$, Nature (London) **453**, 761 (2008).

[6] M. Rotter, M. Tegel, and D. Johrendt, Superconductivity at 38 K in the iron arsenide ($Ba_{1-x}K_x$)$Fe_2As_2$, Phys. Rev. Lett. **101**, 107006 (2008).

[7] X. C. Wang, Q. Q. Liu, Y. X. Lv, W. B. Gao, L. X. Yang, R. C. Yu, F. Y. Li, and C. Q. Jin, The superconductivity at 18 K in LiFeAs system, Solid State Commun. **148**, 538 (2008).

[8] F. C. Hsu, J. Y. Luo, K. W. Yeh, T. K. Chen, T. W. Huang, P. M. Wu, Y. C. Lee, Y. L. Huang, Y. Y. Chu, D. C. Yan, and M. K. Wu, Superconductivity in the PbO-type structure alpha-FeSe, Proc. Natl. Acad. Sci. USA **105**, 14262 (2008).

[9] H. Takahashi, Pressure-induced superconductivity in the iron based ladder material $BaFe_2S_3$, Nat. Mater. **14**, 1008 (2015).

[10] T. Yamauchi, Y. Hirata, Y. Ueda, and K. Ohgushi, Pressure-induced Mott transition followed by a 24-K superconducting phase in $BaFe_2S_3$, Phys. Rev. Lett. **115**, 246402 (2015).

[11] J. Ying, H. Lei, C. Petrovic, Y. Xiao, and V. V. Struzhkin, Interplay of magnetism and superconductivity in the compressed Fe-ladder compound $BaFe_2Se_3$, Phys. Rev. B **95**, 241109(R) (2017).

[12] Y. Nambu, K. Ohgushi, S. Suzuki, F. Du, M. Avdeev, Y. Uwatoko, K. Munakata, H. Fukazawa, S. Chi, Y. Ueda, and T. J. Sato, Block magnetism coupled with local distortion in the iron-based spin-ladder compound $BaFe_2Se_3$, Phys. Rev. B **85**, 064413 (2012).

[13] J. Zhang, X. C. Wang, L. Zhou, G. X. Liu, D. T. Adroja, I. da Silva, F. Demmel, D. Khalyavin, J. Sannigrahi, H. S. Nair, L. Duan, J. F. Zhao, Z. Deng, R. Z. Yu, X. Shen, R. C. Yu, H. Zhao, J. M. Zhao, Y. W. Long, Z. Hu *et al.*, A ferrotoroidic candidate with well-separated spin chains, Adv. Mater. **34**, 2106728 (2022).

[14] J. Zhang, L. Duan, Z. Wang, X. C. Wang, J. F. Zhao, M. L. Jin, W. M. Li, C. L. Zhang, L. P. Cao, Z. Deng, Z. W. Hu, S. Agrestini, M. Valvidares, H. J. Lin, C. T. Chen, J. L. Zhu, and C. Q. Jin, The synthesis of a quasi-one-dimensional iron-based telluride with antiferromagnetic chains and a spin glass state, Inorg. Chem. **59**, 5377 (2020).

[15] J. Zhang, A. C. Komarek, M. Jin, X. C. Wang, Y. T. Jia, J. F. Zhao, W. M. Li, Z. W. Hu, W. Peng, X. Wang, L. H. Tjeng, Z. Deng, R. Z. Yu, S. M. Feng, S. J. Zhang, M. Liu, Y.-F. Yang, H.-j. Lin, C.-T. Chen, X. D. Li *et al.*, High-pressure synthesis, crystal structure, and properties of iron-based spin-chain compound $Ba_9Fe_3Se_{15}$, Phys. Rev. Mater. **5**, 054606 (2021).

[16] J. Zhang, M. Liu, X. C. Wang, K. Zhao, L. Duan, W. M. Li, J. F. Zhao, L. P. Cao, G. Y. Dai, Z. Deng, S. M. Feng, S. J. Zhang, Q. Q. Liu, Y. F. Yang, and C. Q. Jin, $Ba_9V_3Se_{15}$: A novel compound with spin chains, J. Phys.: Condens. Matter **30**, 214001 (2018).

[17] J. Zhang, X. Y. Zhang, Y. H. Xia, J. F. Zhao, L. Duan, G. D. Wang, B. S. Min, H. B. Cao, C. R. Dela Cruz, K. Zhao, H. Y. Sun, J. L. Zhu, J. F. Zhang, T. Xiang, X. C. Wang, and C. Q. Jin, Structure and magnetic properties of $Ba_9V_3Te_{15}$ with ferromagnetic spin chains, Phys. Rev. B **108**, 174423 (2023).

[18] J. Zhang, Y. T. Jia, X. C. Wang, Z. Li, L. Duan, W. M. Li, J. F. Zhao, L. P. Cao, G. Y. Dai, Z. Deng, S. J. Zhang, S. M. Feng, R. Z. Yu, Q. Q. Liu, J. P. Hu, J. L. Zhu, and C. Q. Jin, A new quasi one-dimensional compound $Ba_3TiTe_5$ and superconductivity induced by pressure, NPG Asia Mater. **11**, 60 (2019).

[19] J. Zhang, M. L. Jin, X. Li, X. C. Wang, J. F. Zhao, Y. Liu, L. Duan, W. M. Li, L. P. Cao, B. J. Chen, L. J. Wang, F. Sun, Y. G. Wang, L. X. Yang, Y. M. Xiao, Z. Deng, S. M. Feng,

C. Q. Jin, and J. L. Zhu, Structure-spin-transport anomaly in quasi-1-dimensional $Ba_9Fe_3Te_{15}$ under high pressure, Chin. Phys. Lett. **37**, 087106 (2020).

[20] J. M. Jenks, J. T. Hoggins, L. E. Rendon, S. Cohen, and H. Steinfink, Octahedrally coordinated iron in the Ba-Fe-S system: $Ba_9Fe_3S_{11}(S_2)_2$, a high-pressure polymorph of $Ba_3FeS_5$, Inorg. Chem. **17**, 1773 (1978).

[21] A. C. Larson and R. B. Von Dreele, General structure analysis system (GSAS), Los Alamos National Laboratory Report LAUR (2000), p. 86.

[22] A. Barla, J. Nicolas, D. Cocco, S. Manuel Valvidares, J. Herrero-Martin, P. Gargiani, J. Moldes, C. Ruget, E. Pellegrin, and S. Ferrer, Design and performance of BOREAS, the beamline for resonant x-ray absorption and scattering experiments at the ALBA synchrotron light source, J. Synchrotron Radiat. **23**, 1507 (2016).

[23] X. He, C. L. Zhang, Z. W. Li, S. J. Zhang, B. S. Min, J. Zhang, K. Lu, J. F. Zhao, L. C. Shi, Y. Peng, X. C. Wang, S. M. Feng, J. Song, L. H. Wang, V. B. Prakapenka, S. Chariton, H. Z. Liu, and C. Q. Jin, Superconductivity observed in tantalum polyhydride at high pressure, Chin. Phys. Lett. **40**, 057404 (2023).

[24] X. He, C. L. Zhang, Z. W. Li, K. Lu, S. J. Zhang, B. S. Min, J. Zhang, L. C. Shi, S. M. Feng, Q. Q. Liu, J. Song, X. C. Wang, Y. Peng, L. H. Wang, V. B. Prakapenka, S. Chariton, H. Z. Liu, and C. Q. Jin, Superconductivity discovered in niobium polyhydride at high pressures, Mater. Today Phys. **40**, 101298 (2024).

[25] Q. Q. Liu, X. H. Yu, X. C. Wang, Z. Deng, Y. X. Lv, J. L. Zhu, S. J. Zhang, H. Z. Liu, W. G. Yang, L. Wang, H. K. Mao, G. Y. Shen, Z. Y. Lu, Y. Ren, Z. Q. Chen, Z. J. Lin, Y. S. Zha, and C. Q. Jin, Pressure-induced isostructural phase transition and correlation of FeAs coordination with the superconducting properties of 111-type $Na_{1-x}FeAs$, J. Am. Chem. Soc. **133**, 7892 (2011).

[26] T. Burnus, Z. Hu, H. Wu, J. C. Cezar, S. Niitaka, H. Takagi, C. F. Chang, N. B. Brookes, H.-J. Lin, L. Y. Jang, A. Tanaka, K. S. Liang, C. T. Chen, and L. H. Tjeng, X-ray absorption and x-ray magnetic dichroism study on $Ca_3CoRhO_6$ and $Ca_3FeRhO_6$, Phys. Rev. B **77**, 205111 (2008).

[27] N. Hollmann, Z. Hu, M. Valldor, A. Maignan, A. Tanaka, H. H. Hsieh, H. J. Lin, C. T. Chen, and L. H. Tjeng, Electronic and magnetic properties of the kagome systems $YBaCo_4O_7$ and $YBaCo_3MO_7$ ($M$ = Al, Fe), Phys. Rev. B **80**, 085111 (2009).

[28] C. Y. Kuo, Z. Hu, J. C. Yang, S. C. Liao, Y. L. Huang, R. K. Vasudevan, M. B. Okatan, S. Jesse, S. V. Kalinin, L. Li, H. J. Liu, C. H. Lai, T. W. Pi, S. Agrestini, K. Chen, P. Ohresser, A. Tanaka, L. H. Tjeng, and Y. H. Chu, Single-domain multiferroic $BiFeO_3$ films, Nat. Commun. **7**, 12712 (2016).

[29] J. X. Zhang, Q. He, M. Trassin, W. Luo, D. Yi, M. D. Rossell, P. Yu, L. You, C. H. Wang, C. Y. Kuo, J. T. Heron, Z. Hu, R. J. Zeches, H. J. Lin, A. Tanaka, C. T. Chen, L. H. Tjeng, Y. H. Chu, and R. Ramesh, Microscopic origin of the giant ferroelectric polarization in tetragonal-like $BiFeO_3$, Phys. Rev. Lett. **107**, 147602 (2011).

[30] B. T. Thole, P. Carra, F. Sette, and G. van der Laan, X-ray circular-dichroism as a probe of orbital magnetization, Phys. Rev. Lett. **68**, 1943 (1992).

[31] P. Carra, B. T. Thole, M. Altarelli, and X. Wang, X-ray circular-dichroism and local magnetic-fields, Phys. Rev. Lett. **70**, 694 (1993).

[32] C. J. Wu, B. Chen, X. Dai, Y. Yu, and Z. B. Su, Schwinger-boson mean-field theory of the Heisenberg ferrimagnetic spin chain, Phys. Rev. B **60**, 1057 (1999).

[33] See Supplemental Material at http://link.aps.org/supplemental/10.1103/PhysRevB.111.224405 for the structure parameters from the refinement for the neutron diffraction data collected at 2 K for, the magnetic structure parameters, the irreducible representation, the magnetic structures allowed by the irreducible representation, the temperature dependence of resistance under different pressures, and the pressure dependence of resistance at different fixed temperatures for the second sample.

[34] J. Zhang, X. C. Wang, Y. Q. Hao, G. X. Liu, L. Zhou, D. M. Pajerowski, J. T. Wang, J. L. Zhu, J. Zhao, J. L. Wang, Y. F. Zhao, C. G. Duan, Y. W. Long, C. J. Kang, M. Greenblatt, and C. Q. Jin, Ferroelectricity driven by magnetism in quasi-one-dimensional $Ba_9Fe_3Se_{15}$, arXiv:2207.10834.

[35] L. Duan, X. C. Wang, J. Zhang, J. F. Zhao, W. M. Li, L. P. Cao, Z. W. Zhao, C. J. Xiao, Y. Ren, S. Wang, J. L. Zhu, and C. Q. Jin, Doping effect on the structure and physical properties of quasi-one-dimensional compounds $Ba_9Co_3(Se_{1-x}S_x)_{15}$ ($x = 0 - 0.2$), Chin. Phys. B **30**, 106101 (2021).

[36] T. Graf, D. Mandrus, J. M. Lawrence, J. D. Thompson, P. C. Canfield, S. W. Cheong, and L. W. Rupp, Suppression of the metal-to-insulator transition in $BaVS_3$ with pressure, Phys. Rev. B **51**, 2037 (1995).

[37] L. Forro, R. Gaal, H. Berger, P. Fazekas, K. Penc, I. Kezsmarki, and G. Mihaly, Pressure induced quantum critical point and non-Fermi-liquid behavior in $BaVS_3$, Phys. Rev. Lett. **85**, 1938 (2000).

[38] A. Akrap, V. Stevanovic, M. Herak, M. Miljak, N. Barisic, H. Berger, and L. Forro, Transport and magnetic properties of $BaVSe_3$, Phys. Rev. B **78**, 235111 (2008).

[39] N. D. Mermin and H. Wagner, Absence of ferromagnetism or antiferromagnetism in one- or two-dimensional isotropic Heisenberg models, Phys. Rev. Lett. **17**, 1133 (1966).

[40] J. S. Gardner, M. J. P. Gingras, and J. E. Greedan, Magnetic pyrochlore oxides, Rev. Mod. Phys. **82**, 53 (2010).

[41] L. Balents, Spin liquids in frustrated magnets, Nature (London) **464**, 199 (2010).

[42] H. J. Schulz, Dynamics of coupled quantum spin chains, Phys. Rev. Lett. **77**, 2790 (1996).

[43] I. Tsukada, Y. Sasago, K. Uchinokura, A. Zheludev, S. Maslov, G. Shirane, K. Kakurai, and E. Ressouche, $BaCu_2Si_2O_7$: A quasi-one-dimensional $S = 1/2$ antiferromagnetic chain system, Phys. Rev. B **60**, 6601 (1999).

[44] B. Lake, D. A. Tennant, C. D. Frost, and S. E. Nagler, Quantum criticality and universal scaling of a quantum antiferromagnet, Nat. Mater. **4**, 329 (2005).